ASME Journal of Biomechanical Engineering
Online journal at:
https://asmedigitalcollection.asme.org/biomechanical

Simulation of the Childbirth Process in LS-DYNA

Ru Tao
Department of Mechanical Engineering,
Michigan State University,
East Lansing, MI 48824

Michele J Grimm[1]
Department of Mechanical Engineering,
Michigan State University,
East Lansing, MI 48824;
Department of Biomedical Engineering,
Michigan State University,
East Lansing, MI 48824;
College of Nanotechnology, Science, and Engineering,
University at Albany,
Albany, NY 12222
e-mail: mgrimm@albany.edu

Childbirth or labor, as the final phase of a pregnancy, is a biomechanical process that delivers the fetus from the uterus. It mainly involves two important biological structures in the mother, the uterus—generating the pushing force on the fetus—and the pelvis (bony pelvis and pelvic floor muscles)—resisting the movement of the fetus. The existing computational models developed in this field that simulate the childbirth process have focused on either the uterine expulsion force or the resistive structures of the pelvis, not both. An FEM model including both structures as a system was developed in this paper to simulate the fetus delivery process in LS-DYNA. Uterine active contraction was driven by contractile fiber elements using the Hill material model. The passive portion of the uterus and pelvic floor muscles were modeled with Neo Hookean and Mooney–Rivlin materials, respectively. The bony pelvis was modeled as a rigid body. The fetus was divided into three components: the head, neck, and body. Three uterine active contraction cycles were modeled. The model system was validated based on multiple outputs from the model, including the stress distribution within the uterus, the maximum Von Mises and principal stress on the pelvic floor muscles, the duration of the second stage of the labor, and the movement of the fetus. The developed model system can be applied to investigate the effects of pathomechanics related to labor, such as pelvic floor disorders and brachial plexus injury.
[DOI: 10.1115/1.4064594]

Keywords: childbirth, uterus, pelvis, finite element method, LS-DYNA

1 Introduction

Childbirth is a mechanical process that involves pushing forces—produced by the uterus' active contraction, intra-uterine pressure, and Valsalva (pushing) induced abdominal pressure—that act against a resistance force created by the pelvic structures as the fetus passes through the birth canal [1]. The strong interaction of the uterus, the fetus, and the maternal pelvis results in both the normal cardinal movements of labor and abnormalities of descent. The latter, which can include shoulder dystocia (delay in delivering the shoulders after the head delivers) [2], can lead to a range of injuries to both the infant and the mother [3,4].

Pelvic floor disorders (PFDs), which are a group of pathologies that predominantly become symptomatic in middle-aged and elderly women, are closely related to the fetal delivery process. The typical symptoms of PFDs include urinary incontinence, fecal incontinence, pelvic organ prolapse, and pelvic pain [5]. It is estimated that about one-third of adult women are affected by these conditions to varying degrees [6]. Studies have shown that about 30% to 40% of women suffer from some degree of urinary incontinence during their lifetime [7], and 11% of women have required surgery because of pelvic organ prolapse or urinary incontinence [8]. Childbirth through vaginal delivery has been identified as the primary factor in the development of PFDs [5]. For example, Dimpflet et al. proposed that pelvic floor injuries during childbirth can significantly contribute to the development of PFD [9] because, during delivery of the fetus, the pelvic muscle floor experiences extreme stress and strain conditions that are believed to be the cause of the damage of these key structures. However, understanding of the mechanisms of damage to the pelvic floor is still very limited [10].

Due to clinical, technical, and ethical reasons, in vivo investigation during pregnancy and delivery is very limited. Computational models have been developed to simulate the process of childbirth [11]—but they generally have focused on either the uterine expulsion force or the resistive structures of the pelvis, not both.

For example, several simulation models have been developed to investigate the mechanical interactions of the fetal head and the pelvic muscle floor during the passage of the fetus through the vagina, with the purpose of exploring the mechanisms of PFD [5,12]. Stress and strain fields, reaction forces, and deformation have been calculated and analyzed in these simulations. The geometries commonly include the bones of the pelvis, the pelvic muscle floor, and the fetal head. For the fetal head, some studies used a sphere to represent the structure, while others used more realistic fetal skull geometry obtained from MRI data. The effect of variations in the material properties of the fetal head on the deformation of the pelvic muscle floor has been investigated. A rigid fetal head was found to cause higher stretch and reaction forces in the pelvic floor muscles than a deformable fetal head [13]. The geometries of these structures [14] and the material parameters of the constitutive models [10] for both the pelvic floor muscles and the fetal head have an impact on the calculated results in such simulations. In these models, one of the challenges is to take into account—appropriately and accurately—all forces that act during the fetal delivery process, such as the expelling forces acting on the fetus caused by uterine active contraction. However, in these pelvic models, the uterus and uterine active contraction were not included in the simulations. Instead, the

[1]Corresponding author.
Manuscript received September 18, 2023; final manuscript received January 4, 2024; published online March 25, 2024. Assoc. Editor: Spencer P Lake.

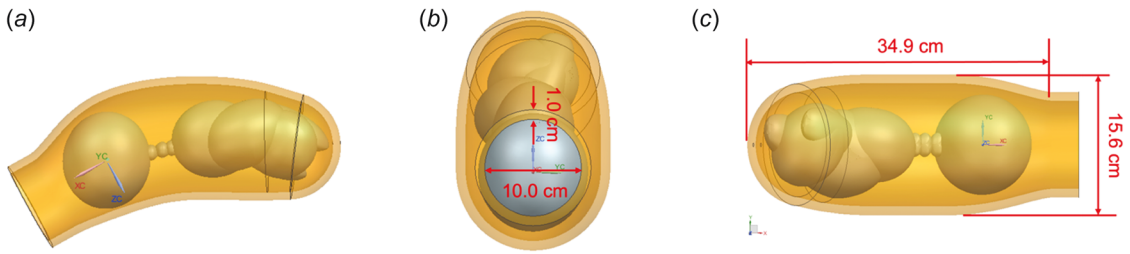

Fig. 1 Geometrical models of the fetus and the uterus

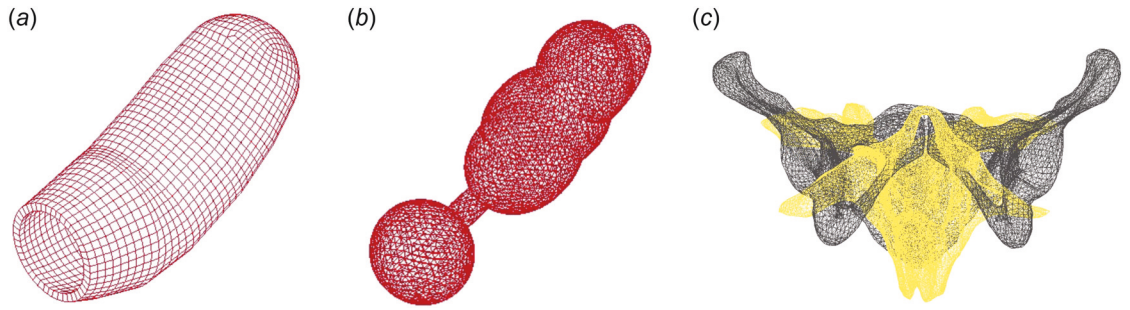

Fig. 2 Mesh of the uterus (*a*), the fetus (*b*), and the pelvis structure (*c*)

fetus's movement or trajectory through the pelvic structures was simulated by applying kinematic boundary conditions to the fetus.

For the uterus-only models simulating uterine active contraction [15,16], most of these models have not considered the strong resistance force caused by the pelvic muscle floor and bony pelvis as the fetus passes through the birth canal during the second stage of labor. For this reason, the calculated deformation, stress and strain field, and other analyses of these uterus-only models are not accurate and reliable.

Therefore, in order to better understand the pathomechanics of the childbirth process and explore the mechanisms of injuries to both the infant and the mother, it is quite important and necessary to model both the structures of the pelvis (bony pelvis and pelvic floor muscles) and the uterus as a system. The objective of this work was to develop a model of maternal tissues that could provide realistic expulsion and resistance forces to govern the movement of an infant through the birth canal and then to use the active contraction of the uterus to deliver a fetal model. Through this study, stresses throughout the maternal and fetal models can be investigated.

2 Materials and Methods

The geometrical models of the uterus and the fetus, shown in Fig. 1, were designed based on experimental data obtained from real-time magnetic resonance imaging of the uterus and fetus during the second stage of labor [17]. The fetus model includes the fetal head, neck, and body. The fetal head was a sphere with a diameter of 80 mm in our initial model analysis, and the length of the whole fetus (with arms and legs tucked against the body) was about 330 mm. The thickness of the uterine wall was set to 10 mm, and the inner diameter of the cervix was 100 mm. The length and maximum width of the uterus was 349 mm and 156 mm.

Meshing of the uterus (Fig. 2(*a*)) and fetus (Fig. 2(*b*)) was done in Hypermesh software using hexahedral elements and tetrahedral elements, respectively, which were then exported to LS-DYNA. There were 3636 nodes and 1795 elements for the uterus structure, and 7694 nodes and 34,087 elements for the fetus.

Since the fibers inside of the uterine wall have a distinct directional organization [18], it was deemed important to model the fibers in three dimensions in the simulation model, not only in two dimensions as has been reported in some previous studies [16]. This allows the effects of fiber orientation on uterus contraction behavior to be investigated. From the mechanics perspective, any direction of force can be divided into three basic forces along the x, y, and z-coordinate axes. So, three directions for the fibers—the longitudinal, circumferential, and normal directions—were created.

Experimental data also shows that the distribution of the fibers changes dramatically in different regions of the uterus [19–21]. In addition, the contraction of the uterus produces a force wave starting from the fundus and propagating to the lower segments of the uterus, with a higher intensity in the fundal region [22]. In order to take such anisotropies and heterogeneities into account to better simulate uterine contraction behavior, the contractile fibers of the longitudinal, circumferential, and normal directions were divided into seven regions for each type of fiber (Fig. 3), while the passive portion of the uterine tissue was constant throughout the model. These seven regions were independent of one another. Figure 3 shows the seven

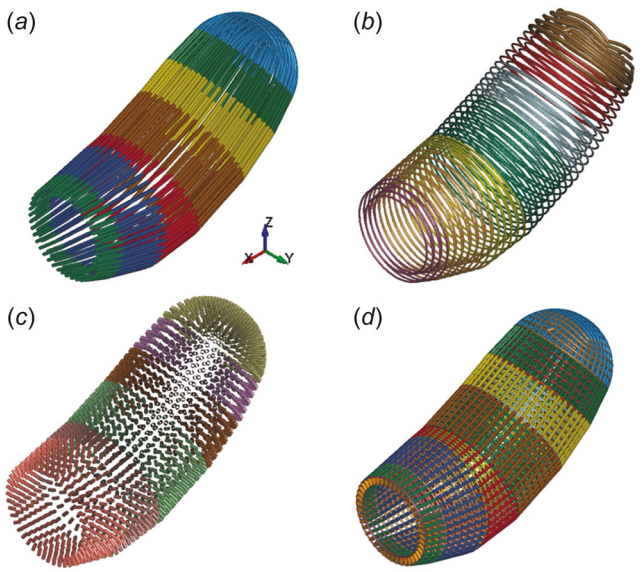

Fig. 3 Contractile fibers inside of the uterine wall: longitudinal (*a*), circumferential (*b*), normal (*c*), and the combination of these three direction fibers (*d*)

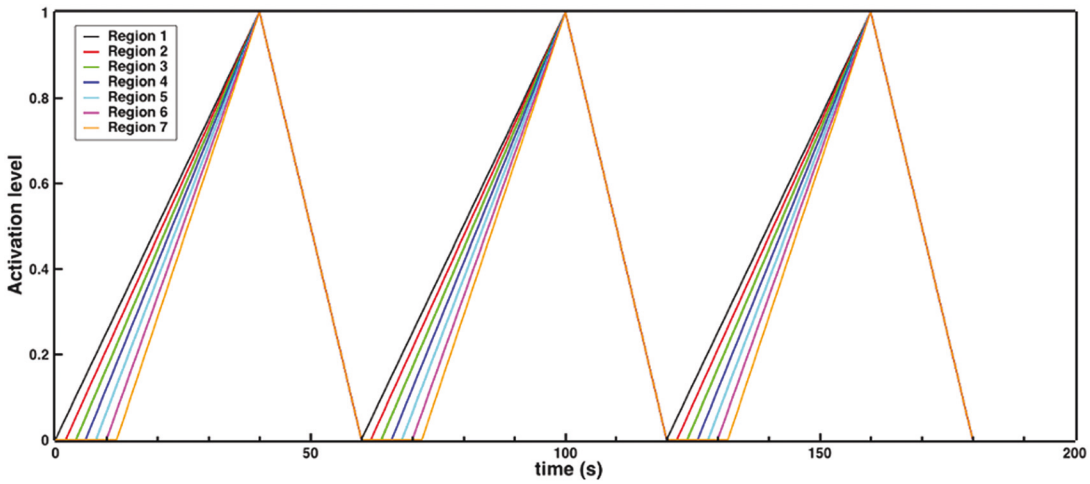

Fig. 4 Activation level curves for seven regions of the contractile fibers. The numbering of the regions goes from the top to the bottom of the uterus. Specifically, region 1 is the fundus (the top region) area, region 7 is the lowest region, and region 2–6 are the regions in the middle.

regions of the longitudinal (Fig. 3(*a*)), circumferential (Fig. 3(*b*)), and normal direction fibers (Fig. 3(*c*)) as well as the combination of all three fiber directions (Fig. 3(*d*)). The longitudinal fibers and the fundal circumferential fibers represented about 40% of the tissue cross-sectional area, while the circumferential fibers in the body of the uterus and the normal fibers throughout comprised about 12% of the tissue cross section perpendicular to the fibers, which was based on experimental data. [18].

The contractile fibers were modeled as truss elements with the Hill material model [23], a one-dimensional model that includes a contractile element, a passive element, and a damping element. The active stress is described as

$$\sigma_a = \sigma_{\max} A(t) F(l) F(v) \tag{1}$$

where $\sigma_{\max}$ is the maximum isometric stress (PIS), $A(t)$ is muscle's activation level, whose value is between zero and one, $F(l)$ is the normalized force-length curve, and $F(v)$ is the normalized force-velocity curve. The normalized force-length curve and force-velocity curve describe fundamental responses of muscle.

The passive element stress, σ_p, is determined by the passive mechanical properties of the muscle. For a hyperelastic material described by the incompressible Mooney–Rivlin model, σ_p was defined first through the equation:

$$W = C_1(\bar{I}_1 - 3) + C_2(\bar{I}_2 - 3) \tag{2}$$

where W is the strain energy density, C_1 and C_2 are material constants, and $\bar{I}_1$ and $\bar{I}_2$ are the first and second invariants of the left Cauchy-Green deformation tensor ($\boldsymbol{B}$). The passive stress in this case is defined by

$$\boldsymbol{\sigma}_{\mathrm{p}} = 2(C_1 + \bar{I}_1 C_2)\boldsymbol{B} - 2C_2\boldsymbol{B}\cdot\boldsymbol{B} - \frac{2}{3}(C_1\bar{I}_1 + 2C_2\bar{I}_2)\boldsymbol{I} \tag{3}$$

For Neo Hookean hyperelastic material, which was used to model the passive responses of the uterine muscle tissue in this study, C_2 equals zero in Eq. (2).

The damping element stress, in LS-DYNA, is defined as

$$\sigma_d = \mathrm{DMP}\frac{l}{l_{\mathrm{orig}}}\dot{\varepsilon} \tag{4}$$

where DMP is the damping coefficient, l is the length of the muscle at a specific time, l_{orig} is the original length of the muscle, and $\dot{\varepsilon}$ is the strain rate. The total stress is the sum of the stress in these three components.

A description of this tissue-level model has been described previously [24]. The normalized force-length curve and force-velocity curve, which describe fundamental responses of muscle and have previously been shown to be appropriate to describe smooth muscle's behavior [25,26], were obtained from the literature [27]. The maximum isometric stress (PIS) was set at 1.2 MPa, and the damping coefficient (DMP) was set equal to 60. The activation level curves for the seven regions were assumed as shown in Fig. 4, where the starting time for region one was at time 0 s. Each of the subsequent regions began contracting 2 s later than the previous region to simulate the propagation of the contraction wave. All of the regions reached a fully activated status and then began to relax synchronously, which was based on the physiologic behavior of the uterus [22]. Three contraction cycles were modeled in this study.

The solid elements for the uterus were coupled with the contractile fibers (truss elements) by sharing the nodes. The passive portion of the uterus, representing the noncontractile portions of the tissue, was modeled as a hyperelastic material with a Neo Hookean model ($C_1 = 0.03$ MPa).

The geometric models of the pelvic bone and pelvic muscle floor, as shown in Figs. 2(*c*), 5(*a*), and 5(*b*), were created based on the in vivo MR images of a 21-year-old woman at the gestational stage

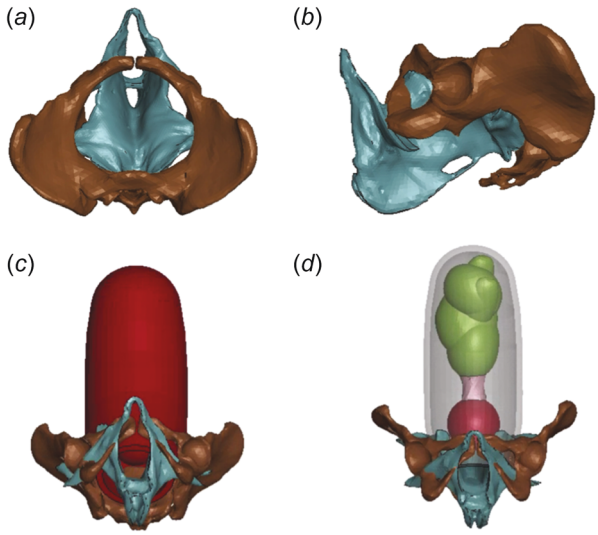

Fig. 5 The geometries of the bony pelvis, pelvic muscle floor, fetus, and the uterus

of 35 weeks and 6 days. The pelvic bone included the sacrum, the pubic symphysis of the bony pelvis, and the innominate bones. The pelvic muscle floor included the levator ani, coccygeus, and the superficial perineal muscles and perineal membrane [28,29]. They were imported into Hypermesh to construct the mesh. Triangular shell elements, with an average element size of 5 mm and a thickness of 1 mm were used for the maternal bony pelvis. Tetrahedral elements, with an average size of 4 mm, were used for the pelvic floor muscles. In total, the finite element mesh of the pelvic structures was composed of 80,675 tetrahedral elements, 14,454 triangular elements, and 27,436 nodes, as shown in Fig. 2(*c*). The bony pelvis was modeled as a rigid body. The pelvic muscle floor was modeled as a hyperelastic material with a Mooney–Rivlin model ($C_1 = 0.016$ MPa, and $C_2 = 0.004$ MPa) [12].

The fetus was modeled as three components—head, neck, and body—where the fetal head was a rigid body, the neck was elastic (E = 50 MPa, v = 0.49), and the body was Neo Hookean hyperelastic ($C_1 = 0.07$ MPa [30]). The contact between the fetus and both the uterus and pelvic structures was modeled as a surface-to-surface contact. No external loads were applied. The material properties of the passive portion of the uterus, the fetus, and the pelvic structures are summarized in Table 1.

For the boundary conditions, the cervix (Fig. 6(*a*)) and bony pelvis were fixed in the x, y, and z translation directions in space. The nodes with colors on the pelvic floor muscles (Fig. 6(*b*)) were fixed as well.

The active contraction of the uterus was implemented, and the resulting movement of the fetal model through the pelvis was observed. In addition, the stress developed within the pelvic floor muscles and fetal neck and body were analyzed.

The simulation results were reviewed to verify that the model was acting as expected. The model was then validated by comparing the simulation results with other childbirth modeling and experimental results in the literature, with details in the Results and Discussion Sections.

After validation, the effects of the size of the fetal head on the mechanical response (the Von Mises stress and maximum principal stress) of the uterus, fetal neck, and pelvic floor were investigated. Two fetal head sizes, 80 mm and 90 mm, were used. Three elements—in the uterine fundus, fetal neck, and pelvis floor muscles, respectively—were chosen as key indicators of the response of the structures (see Fig. S1 available in the Supplemental Materials on the ASME Digital Collection).

Table 1 Material properties for the uterus, fetus, and the pelvic structures

Parts		Material properties
Uterus (passive component)		Neo Hookean (C_1= 0.03 MPa) [30]
Fetus	Head	Rigid body
	Neck	Elastic (E = 50 MPa)
	Body	Neo Hookean (C_1 = 0.07 MPa) [30]
Pelvic structures	Bony pelvis	Rigid body
	Pelvic floor muscles	Mooney–Rivlin (C1= 0.016 MPa C_2= 0.004 MPa) [12]

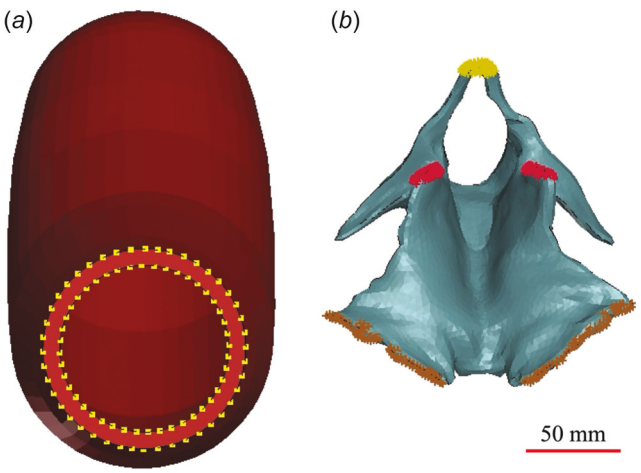

Fig. 6 Boundary conditions of the cervix (*a*) and the pelvic floor muscles (*b*). A scale bar of 50 mm is provided.

3 Results and Discussion

3.1 Model Verification and Validation. Verification focused on two portions of the model: the uterus and the fetus. For the uterus, we examined whether the contractile behavior resembled normal physiology. For the fetus, we focused on whether the fetus would remain in a vertex presentation and descend through the maternal pelvis. Both of these expected behaviors were confirmed. The simulation results showing contraction of the uterus are provided in Fig. 7. The uterus started to contract from the fundus region, and the contraction wave started to propagate to the lower part once the uterus was activated. By t = 30 s, all regions contracted, and the largest stress was 0.05 MPa at the top of the fundus area (Fig. 7(*b*)). By t = 50 s, the stress for the different regions within the uterus each reached their maximum value for the first contraction (Fig. 7(*c*)), and then decreased slightly due to the decrease of the activation level in the first cycle—allowing relaxation of the uterus. After that, the stress increased again in the second contraction. The maximum stress for different regions within the uterus in the second cycle (Fig. 7(*d*)) was higher than that in the first cycle (Fig. 7(*c*)).

The model was validated through comparisons with both experimental and simulation results in the literature. Specifically, the largest stress within the uterus was always in the fundus region, which agrees with experimental results that show that the fundus has a higher contraction intensity than the middle and lower parts of the uterus [22]. The values of maximum Von Mises and principal stress within the pelvic floor muscles also agreed well with other researchers' simulation results [5]. In addition, the duration time of the labor, the displacement of the fetus during the delivery, and the rotation of the fetus were all within clinically observed ranges. The details of validation comparisons are summarized in Table 2 and are discussed in more detail in subsequent paragraphs of the Results.

The Von Mises stresses for the pelvic floor muscles are shown in Fig. 8. At time = 30 s, the largest stress of the pelvic floor muscles was 0.03 MPa (Fig. 8(*b*)). As the fetus continued to move forward, the stress within the pelvic floor muscles became much larger. At time = 50 s, the largest stress was 0.06 MPa (Fig. 8(*c*)). The maximum Von Mises stress was 0.11 MPa at 98 s, occurring at the midpoint in the second cycle, right before the fetal head was delivered (Fig. 8(*d*)). The maximum principal stress was 0.12 MPa at an element in the centerline of the pelvic floor muscles. To validate the simulation results of the pelvis structure, the values of the Von Mises stress and the maximum principal stress were compared with similar modeling work where the stresses of the pelvis floor muscles were analyzed when the fetal head passed through [5]. Specifically, in their work, the maximum Von Mises stress and maximum principal stress were 0.149 MPa and 0.117 MPa, respectively, for the 80 mm fetal head case [5]. In comparison with their work, the values from the current model for Von Mises stress (0.11 MPa) and maximum principal stress (0.12 MPa) of the pelvis floor muscles are very close to their results.

The fetal displacement with time during the delivery process is shown in Fig. 9. The contraction of the uterus pushed the fetus forward through the pelvic structures. The fetus naturally rotated in a clockwise direction in the sagittal plane of the pelvis as it moved through the birth canal. The outward displacement continued to increase until 50 s in the first contraction, then decreased slightly in the first recovery phase, and increased again in the second

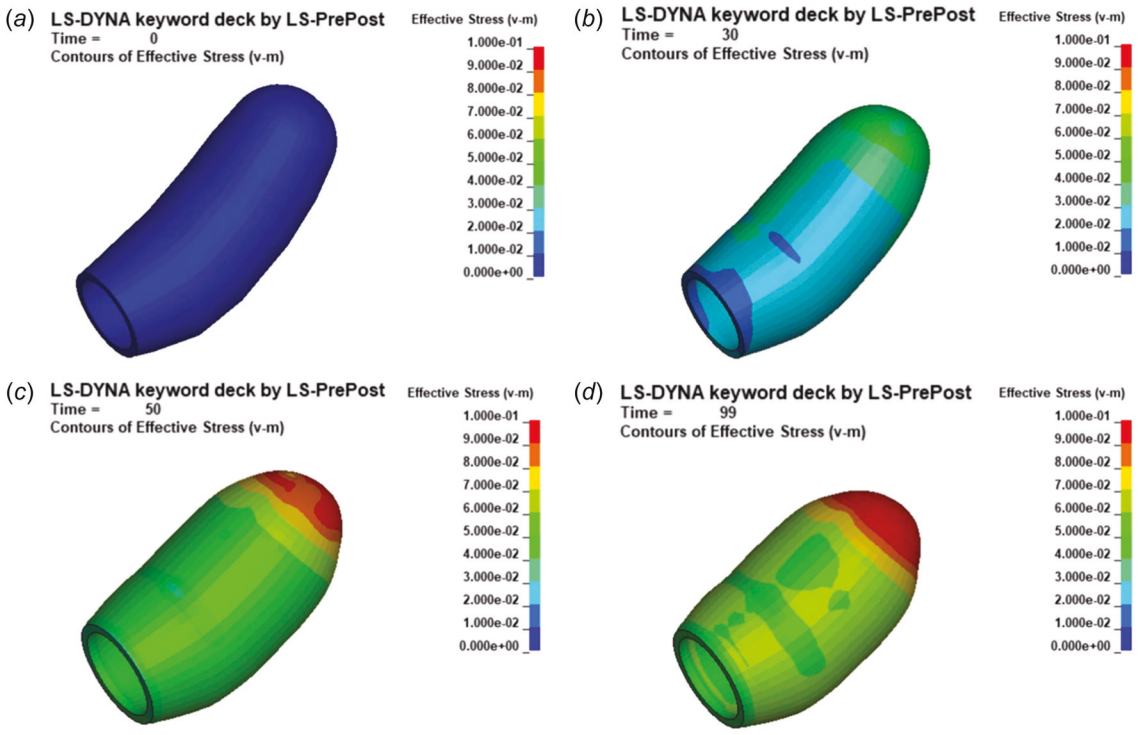

Fig. 7 Representation of the deformation and stress of the uterus at times of 0 s (*a*), 30 s (*b*), 50 s (*c*), and 99 s (*d*). These were determined for the full model anatomy, including the pelvis and fetus.

Table 2 Summaries of the validations

Biological structure	Index for validation	Simulation results	Validation source	Reference
Uterus	Stress distribution	Stresses in fundus region was higher than that of lower regions	Contraction was stronger in the fundus region than the lower regions	[22]
Pelvis floor muscles	Von Mises stress	0.11 MPa	0.149 MPa	[5]
	Maximum principal stress	0.12 MPa	0.117 MPa	[5]
Fetus	Delivery time	100 s	2—200 min	[31]
	Rotation angle	46 deg	45 deg	[32]

contraction cycle. The fetal head was delivered during the second contraction. The overall displacement of the fetus during the delivery process was about 320 mm. The delivery time of the fetus in the model was validated in comparison to clinical data. In clinical deliveries, the duration for the second stage of labor varies significantly—from 2 min to 200 min [31]. In this current version of the model, it took 100 s for the fetus to deliver, which was close to that lower bound of 2 min. While this represents an extremely precipitous delivery—a second stage that includes only two contractions—the displacement of the fetus within the birth canal and pelvis is representative of the normal clinical movement. More importantly, by increasing the damping coefficient (DMP) value within the Hill model, the delivery process can be slowed down and the number of contractions and time of the second stage can be increased.

Figure 10 shows the rotation of the fetus during the labor, and this is the rotation angle that was used as an index for validation. By comparing the initial and the last position of the fetus, the spine of the model fetus rotated 46 deg within the mother's sagittal plane, which is quite close to the fetus' rotation angle of approximately 45 deg during the cardinal movements of labor that span from the completion of internal rotation to the end of restitution [32]. The rotation in this model is solely the result of the interaction of the fetus with the bone and soft tissue structures of the pelvis—it was not prescribed.

The stress experienced by the fetus during the delivery process is also shown in Fig. 10. The overall stress within the fetus increased until 50 s (Fig. 10(*c*)), then decreased in the first recovery phase (Fig. 10(*d*)), and finally continued to increase again in the second contraction cycle until the delivery of the head (Fig. 10(*f*)). The stress was concentrated in the fetus' neck and was much larger than the stress predicted within the fetus' body.

3.2 Parametric Analysis. The results of the parametric analysis of the effects of fetal head size on stresses in the uterus, fetal neck, and pelvic floor muscles are shown in Fig. 11 and Table 3. Two diameters of the fetal head, 80 mm, and 90 mm, were chosen based on the normal size of a fetal head during labor, and this choice was supported by its alignment with other studies presented in the literature [5]. The Von Mises stress and maximum principal stress in the fetal neck increased significantly (48.2% and 41.4%) with the increase in the fetal head size from 80 mm to 90 mm. Both stresses in the pelvic floor muscles also increased slightly (Von Mises: +11.4%; maximum principal: +27.3%) with the increase in the head size. Conversely, the size of the fetal head had almost no impact on the stresses of the uterus. As the stress in the uterus is primarily created by the active contraction of the tissue, and not as a result of a reaction to the interaction of the uterus with the fetus, this last result meets expectations.

In previous work published by Xuan that examined stress in the pelvic floor muscles for different sizes of fetal head, the increase in

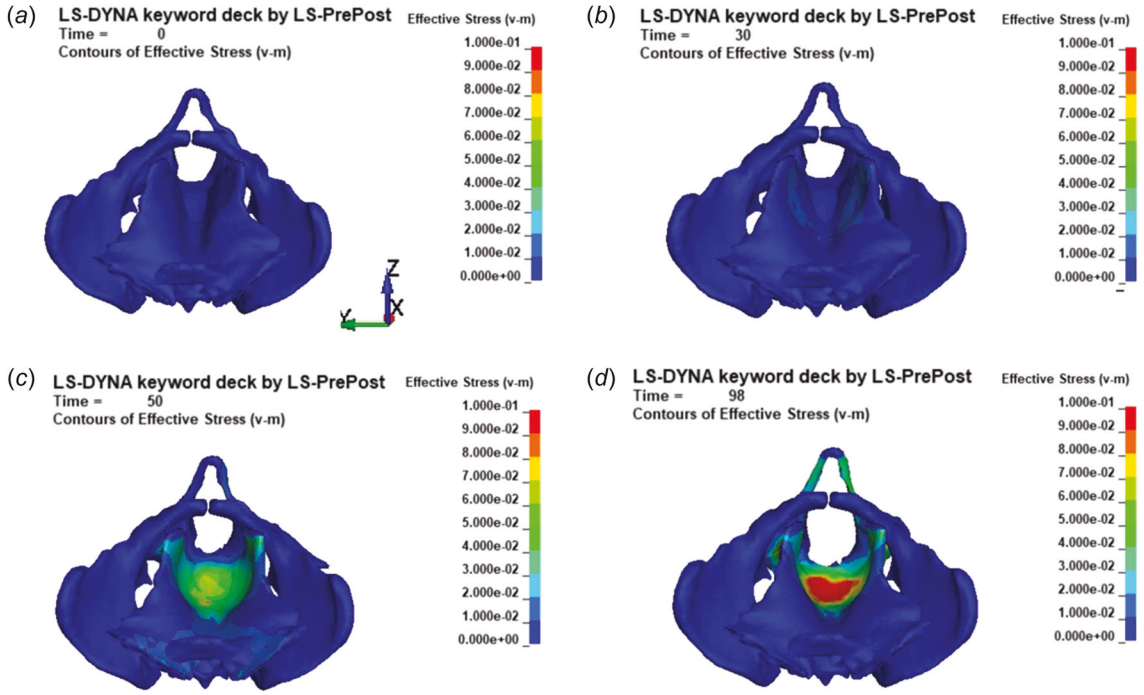

Fig. 8 Stress nephogram of the pelvis muscle floor at times of 0 s (*a*), 30 s (*b*), 50 s (*c*), and 98 s (*d*)

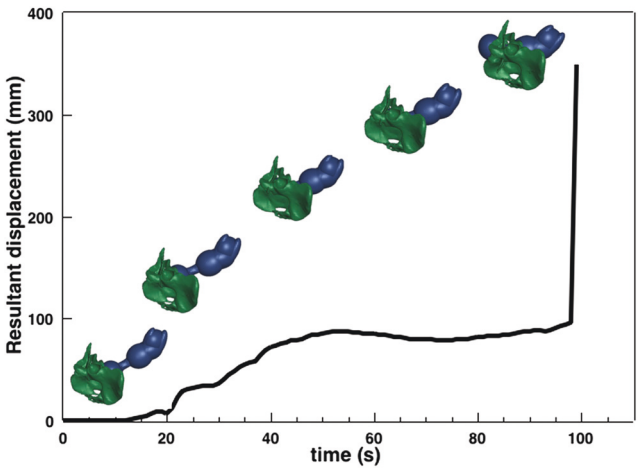

Fig. 9 Displacement of fetus during the delivery process

both the Von Mises stress and maximum principal stress within the pelvic floor muscles increased by a much greater degree (Von Mises: +33.3%; maximum principal: +58.3%) as the fetal head diameter increased from 80 to 90 mm [5], which is different from our work. One explanation for this difference is that, in Xuan's model, there was only a fetal head modeled as a rigid sphere. In contrast, a deformable fetal neck and body were modeled in the current work. The deformation and bending of the fetal neck and body during labor in the current model dissipated some of the energy needed to push and deliver the larger fetal head—thus reducing the energy transmitted to the pelvic floor muscles and reducing their stress. This is demonstrated through the significant increase in the stresses in the fetal neck, as shown in Fig. 11, with the larger fetal head.

The size of the fetal head also plays an important role in regulating the delivery time. Clinical research has already shown that a larger fetal head makes the delivery process more difficult and can cause prolonged labor [33,34]. This can be predicted and analyzed by the simulation model system. The fetal head with an 80 mm diameter was completely delivered at 99 s, while the fetal head with a 90 mm diameter was just partially delivered at this time, which means that a longer delivery time was required. With the larger fetal head, the resistance force experienced by the fetus will be increased. Evidence for this is shown in the increased stresses that occur in the pelvic floor muscles for the larger fetal head. Therefore, it is more difficult for the fetus with the larger head to move through the birth canal. As a result, more uterine contraction cycles are required, so that the delivery time will be increased.

3.3 Limitations of the Model. As always, there are limitations with the model described here—which do present opportunities for future research. First, the structures of the uterus, the bony pelvis, and the pelvic floor muscles are coupled tightly through connective tissues in a woman's body. However, in this model system, these structures were put in their relative positions by applying boundary conditions for each of them. This may affect the stress developed within the tissues—in particular, the pelvic floor muscles, which deform significantly and will react to deformation in adjacent tissues. The incorporation of such connective tissues and surrounding organs, such as the vagina, the rectum, and the bladder, will negatively impact computational time due to the increase in the computation amount. The model as described in this paper already required 14 days for each run. If these structures are included, however, the forces resisting the movement of the fetus and the stresses experienced by the fetus will increase, and the stress value and distribution among the pelvis floor muscles will also be adjusted and more accurate. Most models investigating the mechanical behaviors of pelvis floor muscles have not considered such connective tissues, while they have also lacked the uterus and uterine active contraction [5,13,35]. In the previous studies, the movement of the fetus was imposed as a specific trajectory. The model in this study was able to push the fetus through the birth canal due to the uterine active contraction. Also, in the majority of previous models, only the fetal head was included, typically as a sphere or based on real skull geometry from MRI images [5,36,37], and only one contact between the fetal head and the pelvic floor muscles was defined. The model in this study introduced a whole fetus, including the head, neck, and body. The added biological

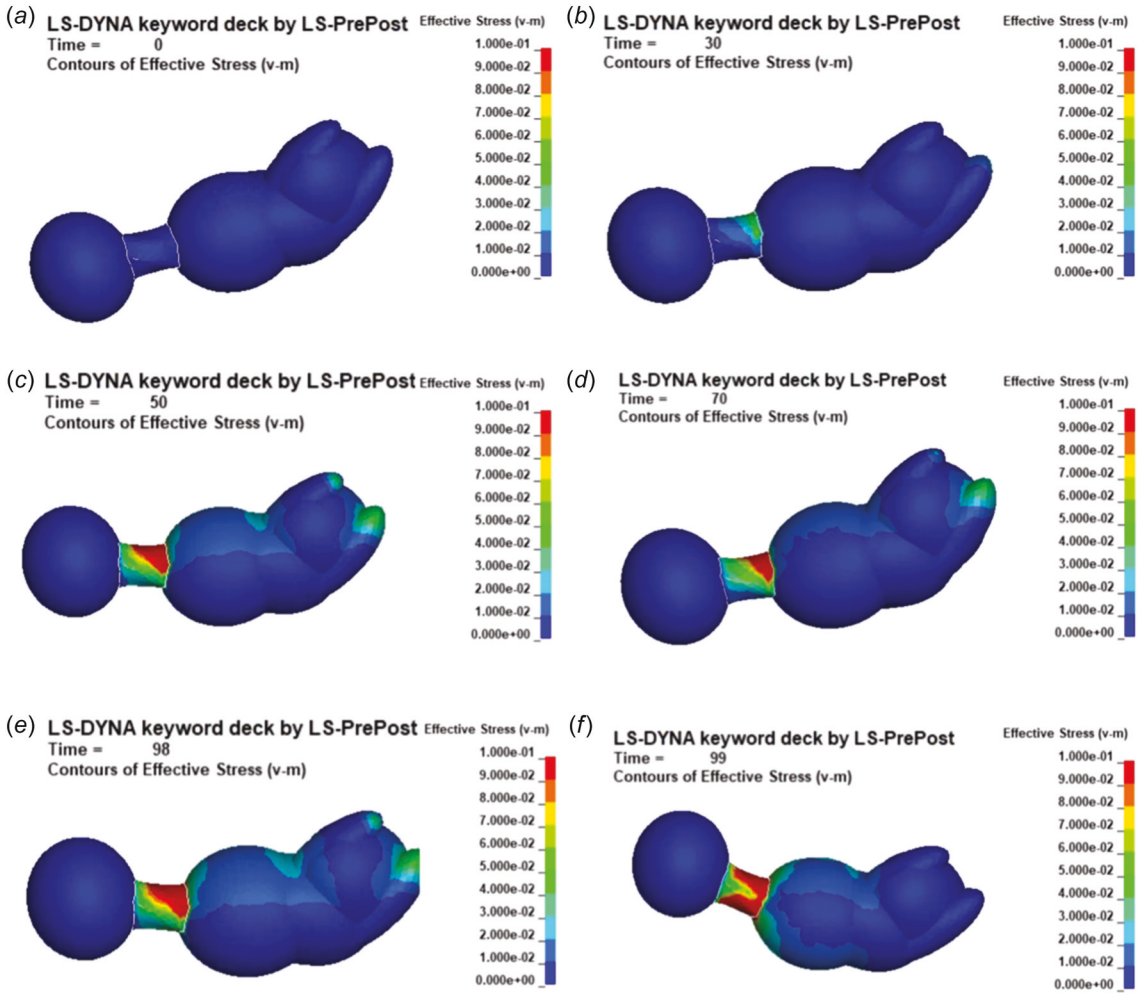

Fig. 10 Stress nephogram of the fetus during the delivery process from 0 (*a*), 30 (*b*), 50 (*c*), 70 (*d*), 98 (*e*), and 99 (*f*) seconds

structures of the uterus and fetal body, as well as defining and calculating responses for more contacts in this study, increased the number of needed computations and required longer computation time.

For the contractile fibers, the current model was able to represent the main characteristics of fiber distribution within the uterus, as identified through experiments. For example, the fiber distribution for human uterine tissue showed: strong anisotropy and heterogeneity between different regions—with higher fiber content in the fundus region [22]; longitudinal and circumferential directions as the two main fiber directions [20]; and fibers that are inclined with respect to the uterine wall, which means they have a three-dimensional fiber arrangement [18]. Although this model will allow for easy adjustment of the distribution of fibers within the different regions as the three fiber directions were modeled separately, the distribution of the fibers in this version of the model was constant within the middle and lower parts of the uterus (regions 2–7). More experimental data based on high-resolution images of the variation in orientation and statistics regarding fiber content will be needed in order to model the fibers more accurately in these regions.

The uterine active contraction in this model was described using the phenomenological Hill model, which has been used to model other smooth muscle tissues or organs in literature [25,38,39]. The Hill model has been shown to successfully match the macroscale mechanical behavior of muscles found through phenomenological experiments. However, there is no underlying biological or chemical mechanisms at the cellular or subcellular level included in the phenomenological Hill model to describe the activation of the muscle contraction. Therefore, it cannot be used to investigate the effects of cellular-level biochemical behaviors on the tissue and organ-level behaviors. A few efforts have been made to include the cross-bridge sliding [40,41] or calcium dynamics [42,43] within the Hill model in order to generate the active force and then incorporate that active component with a three-dimensional passive component of the muscle within the framework of continuum mechanics theory to develop a multiscale model. This has not been attempted in the current project but could be integrated in the future.

Finally, the intra-uterine pressure is the hydrostatic pressure caused within the fluid inside the uterus. It is unclear how important the intra-uterine pressure is for the delivery process. Many women who experience spontaneous rupture of their membranes have a labor that progresses without delay or complication; however, there is generally some volume of fluid that remains within the uterus. Evidence for this comes both from the ability to measure intra-uterine pressure with a catheter during labor after the membranes have ruptured and the gush of fluid that often accompanies the delivery of the infant's body. None of the current models of labor and delivery, whether computational or physical models, include this feature. This question can be explored in the future by including hydrostatic pressure within the model system.

4 Conclusion

In conclusion, an FEM model system was developed in LS-DYNA to simulate the uterine cyclic active contraction and delivery of a deformable fetus through the bony pelvis and pelvic floor

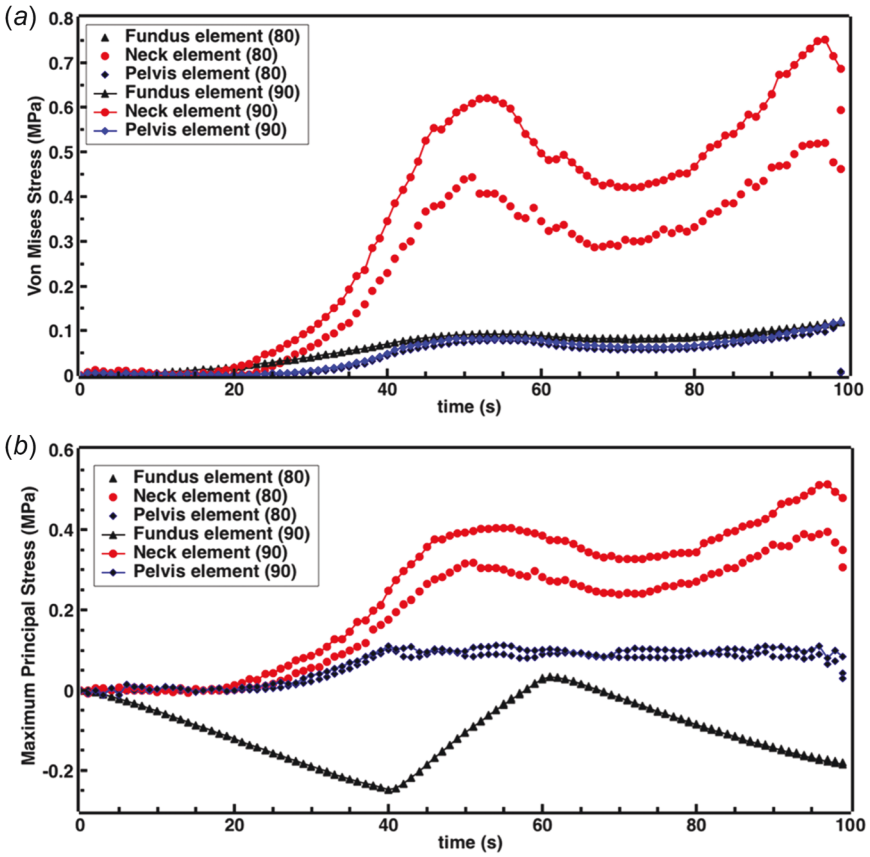

Fig. 11 Effects of size of the fetal head on Von Mises stress (*a*) and maximum principal stress (*b*) of the uterus, fetal neck, and pelvic floor muscles. Stress values were assessed in a single indicator element within each of the three anatomical structures.

Table 3 Maximum stresses are seen in an indicator element for the uterus, fetal neck, and pelvic floor muscles—comparing 80 mm and 90 mm fetal head sizes

	80 mm Head				90 mm Head			
	Max Von Mises Stress (MPa)	Time point (s)	Max principal stress (MPa)	Time point (s)	Max Von Mises stress (MPa)	Time point (s)	Max principal stress (MPa)	Time point (s)
Uterus	0.12	99	−0.24	40	0.12	99	−0.25	40
Pelvic floor	0.11	98	0.09	96	0.12	99	0.11	96
Fetal neck	0.6	99	0.4	97	0.75	97	0.51	97

muscles. In this model, the uterus was able to perform the large deformation, cyclic active contraction, and propagation of the contraction wave needed to achieve delivery. During the childbirth process, the greatest stresses for the pelvic floor muscles happened in the contact area with the fetus's head. For the fetus, the delivery displacement increased significantly and then decreased slightly with the rise and the decline of the activation level in different contractions, respectively. The fetal neck had much higher stress compared to the stress in the fetus' body. The larger fetal head was found to increase the stresses in the fetal neck significantly, while it had smaller effect on stresses in the pelvic floor muscles and a minimal effect on the uterus. This model matches the phenomenological activity of the uterus and the response of the fetus to that activity. This is the first model that has relied on force derived directly from uterine contractions to deliver a full fetal body through the maternal pelvis. The model system will be used in the future for analysis of tissue response linked to pelvic floor disorders and brachial plexus injury.

Funding Data

- National Science Foundation (Grant No. CBET-2028474; Funder ID: 10.13039/100000001).

Data Availability Statement

The datasets generated and supporting the findings of this article are obtainable from the corresponding author upon reasonable request.

References

[1] Grimm, M. J., 2021, "Forces Involved With Labor and Delivery—A Biomechanical Perspective," Ann. Biomed. Eng., **49**(8), pp. 1819–1835.

[2] Acker, D. B., Sachs, B. P., and Friedman, E. A., 1985, "Risk Factors for Shoulder Dystocia," Obstet. Gynecol., **66**(6), pp. 762–768.

[3] Doumouchtsis, S. K., and Arulkumaran, S., 2009, "Are All Brachial Plexus Injuries Caused by Shoulder Dystocia?" Obstet. Gynecol. Surv., **64**(9), pp. 615–623.

[4] Mitanchez, D., 2010, "Foetal and Neonatal Complications in Gestational Diabetes: Perinatal Mortality, Congenital Malformations, Macrosomia, Shoulder Dystocia, Birth Injuries, Neonatal Complications," Diabetes Metab., **36**(6), pp. 617–627.

[5] Xuan, R., Yang, M., Gao, Y., Ren, S., Li, J., Yang, Z., Song, Y., Huang, X. H., Teo, E. C., Zhu, J., and Gu, Y., 2021, "A Simulation Analysis of Maternal Pelvic Floor Muscle," Int. J. Environ. Res. Public Health, **18**(20), p. 10821.

[6] Paulo, M. P. L., 2008, "Biomechanics of the Pelvic Floor During Vaginal Delivery," Doctoral dissertation, Universidade do Porto, Porto, Portugal.

[7] Lien, K.-C., Morgan, D. M., Delancey, J. O. L., and Ashton-Miller, J. A., 2005, "Pudendal Nerve Stretch During Vaginal Birth: A 3D Computer Simulation," Am. J. Obstet. Gynecol., **192**(5), pp. 1669–1676.

[8] Olsen, A. L., Smith, V. J., Bergstrom, J. O., Colling, J. C., and Clark, A. L., 1997, "Epidemiology of Surgically Managed Pelvic Organ Prolapse and Urinary Incontinence," Obstet. Gynecol., **89**(4), pp. 501–506.

[9] Dimpfl, T., Jaeger, C. H., Mueller-Felber, W., Anthuber, C., Hirsch, A., Brandmaier, R., and Schuessler, B., 1998, "Myogenic Changes of the Levator Ani Muscle in Premenopausal Women: The Impact of Vaginal Delivery and Age," Neurourol. Urodyn. Official J. Int. Continence Soc., **17**(3), pp. 197–205.

[10] Parente, M. P. L., Jorge, R. M. N., Mascarenhas, T., Fernandes, A. A., and Martins, J. A. C., 2009, "The Influence of the Material Properties on the Biomechanical Behavior of the Pelvic Floor Muscles During Vaginal Delivery," J. Biomech., **42**(9), pp. 1301–1306.

[11] Chen, S., and Grimm, M. J., 2020, "Childbirth Computational Models: Characteristics and Applications," ASME J. Biomech. Eng., **143**(**5**), p. 050801.

[12] Teixeira Da Silva, M. E., 2017, "Faculdade De Engenharia Da Universidade Do Porto Evaluating the Mechanical Properties of Biological Soft Tissues Using Inverse Methods: Application to the Pelvic Floor Muscles," Doctoral dissertation, Universidade do Porto, Porto, Portugal.

[13] Silva, M. E. T., Oliveira, D. A., Roza, T. H., Brandão, S., Parente, M. P. L., Mascarenhas, T., and Natal Jorge, R. M., 2015, "Study on the Influence of the Fetus Head Molding on the Biomechanical Behavior of the Pelvic Floor Muscles, During Vaginal Delivery," J. Biomech., **48**(9), pp. 1600–1605.

[14] Lepage, J., Jayyosi, C., Lecomte-Grosbras, P., Brieu, M., Duriez, C., Cosson, M., and Rubod, C., 2015, "Biomechanical Pregnant Pelvic System Model and Numerical Simulation of Childbirth: Impact of Delivery on the Uterosacral Ligaments, Preliminary Results," Int. Urogynecol. J. Pelvic Floor Dysfunct., **26**(4), pp. 497–504.

[15] Sharp, G. C., Saunders, P. T. K., and Norman, J. E., 2013, "Computer Models to Study Uterine Activation at Labour," Mol. Hum. Reprod., **19**(11), pp. 711–717.

[16] Vila Pouca, M. C. P., Ferreira, J. P. S., Oliveira, D. A., Parente, M. P. L., Mascarenhas, M. T., and Natal Jorge, R. M., 2019, "Simulation of the Uterine Contractions and Foetus Expulsion Using a Chemo-Mechanical Constitutive Model," Biomech. Model Mechanobiol., **18**(3), pp. 829–843.

[17] Bamberg, C., Rademacher, G., Güttler, F., Teichgräber, U., Cremer, M., Bührer, C., Spies, C., Hinkson, L., Henrich, W., Kalache, K. D., and Dudenhausen, J. W., 2012, "Human Birth Observed in Real-Time Open Magnetic Resonance Imaging," Am. J. Obstet. Gynecol., **206**(6), pp. 505-e1–505.e6.

[18] McLean, J. P., Fang, S., Gallos, G., Myers, K. M., and Hendon, C. P., 2020, "Three-Dimensional Collagen Fiber Mapping and Tractography of Human Uterine Tissue Using OCT," Biomed. Opt. Express, **11**(10), p. 5518.

[19] Fang, S., McLean, J., Shi, L., Vink, J. S. Y., Hendon, C. P., and Myers, K. M., 2021, "Anisotropic Mechanical Properties of the Human Uterus Measured by Spherical Indentation," Ann. Biomed. Eng., **49**(8), pp. 1923–1942.

[20] Fiocchi, F., Nocetti, L., Siopis, E., Currà, S., Costi, T., Ligabue, G., and Torricelli, P., 2012, "In Vivo 3T MR Diffusion Tensor Imaging for Detection of the Fibre Architecture of the Human Uterus: A Feasibility and Quantitative Study," Br. J. Radiol., **85**(1019), pp. e1009–e1017.

[21] Zhang, W., and Chen, J., 2020, "Diffusion Tensor Imaging (DTI) of the Cesarean-Scarred Uterus In Vivo at 3T: Comparison Study of DTI Parameters Between Nonpregnant and Pregnant Cases," J. Magn. Reson. Imaging, **51**(1), pp. 124–130.

[22] Caldeyro-Barcia, R., Alvarez, H., and Poseiro, J. J., 1955, "Normal and Abnormal Uterine Contractility in Labour," Triangle, **2**(41).

[23] Hill, A. V., 1938, "The Heat of Shortening and the Dynamic Constants of Muscle," Proc. R. Soc. London. Ser. B-Biol. Sci., **126**(843), pp. 136–195.

[24] Tao, R., and Grimm, M., 2022, "Simulation of Three-Dimensional Involuntary Muscle Active Contraction Using a Hill Constitutive Model in LS-DYNA," Ninth World Congress of Biomechanics, Taipei, Taiwan, July 10–14, p. 0706.

[25] Bates, J. H. T., and Lauzon, A.-M., 1912, "Parenchymal Tethering, Airway Wall Stiffness, and the Dynamics of Bronchoconstriction," J. Appl. Physiol., **102**(5), pp. 1912–1920.

[26] Murphy, R. A., 1988, "Muscle Cells of Hollow Organs," Physiology, **3**(3), pp. 124–128.

[27] Östh, J., 2014, *Muscle Responses of Car Occupants: Numerical Modeling and Volunteer Experiments Under Pre-Crash Braking Conditions*, Chalmers Tekniska Hogskola, Gothenburg, Sweden.

[28] Routzong, M. R., Moalli, P. A., Rostaminia, G., and Abramowitch, S. D., 2023, "Morphological Variation in the Pelvic Floor Muscle Complex of Nulliparous, Pregnant, and Parous Women," Ann. Biomed. Eng., **51**(7), pp. 1–10.

[29] Chen, S., Routzong, M. R., Abramowitch, S. D., and Grimm, M. J., 2023, "A Computational Procedure to Derive the Curve of Carus for Childbirth Computational Modeling," ASME J. Biomech. Eng., **145**(1), p. 011002.

[30] Buttin, R., Zara, F., Shariat, B., Redarce, T., and Grangé, G., 2013, "Biomechanical Simulation of the Fetal Descent Without Imposed Theoretical Trajectory," Comput. Methods Programs Biomed., **111**(2), pp. 389–401.

[31] Abalos, E., Oladapo, O. T., Chamillard, M., Díaz, V., Pasquale, J., Bonet, M., Souza, J. P., and Gülmezoglu, A. M., 2018, "Duration of Spontaneous Labour in 'Low-Risk' Women With 'Normal' Perinatal Outcomes: A Systematic Review," Eur. J. Obstet. Gynecol. Reproductive Biol., **223**, pp. 123–132.

[32] Ghi, T., Farina, A., Pedrazzi, A., Rizzo, N., Pelusi, G., and Pilu, G., 2009, "Diagnosis of Station and Rotation of the Fetal Head in the Second Stage of Labor With Intrapartum Translabial Ultrasound," Ultrasound Obstet. Gynecol., **33**(3), pp. 331–336.

[33] Korhonen, U., Taipale, P., and Heinonen, S., 2014, "The Diagnostic Accuracy of Pelvic Measurements: Threshold Values and Fetal Size," Arch. Gynecol. Obstet., **290**(4), pp. 643–648.

[34] Elvander, C., Högberg, U., and Ekeus, C., 2012, "The Influence of Fetal Head Circumference on Labor Outcome: A Population-Based Register Study," Acta Obstet. Gynecol. Scand., **91**(4), pp. 470–475.

[35] Parente, M. P. L., Jorge, R. M. N., Mascarenhas, T., Fernandes, A. A., and Martins, J. A. C., 2008, "Deformation of the Pelvic Floor Muscles During a Vaginal Delivery," Int. Urogynecol. J., **19**(1), pp. 65–71.

[36] Da Silva, M. E. T., Parente, M. P. L., and Jorge, R. M. N., 2013, "Biomechanical Study of a Fetus During a Vaginal Delivery," Third Portuguese Bioengineering Meeting, ENBENG 2013 - Book of Proceedings, Braga, Portugal, Feb. 20–23.

[37] Li, X., Kruger, J. A., Chung, J.-H., Nash, M. P., and Nielsen, P. M. F., 2008, "LNCS 5242 - Modelling Childbirth: Comparing Athlete and Non-Athlete Pelvic Floor Mechanics," Med. Image Comput. Comput. Assist. Interv., **11**(Pt 2), pp. 750–757.

[38] Pavan, P. G., Todros, S., Pachera, P., Pianigiani, S., and Natali, A. N., 2019, "The Effects of the Muscular Contraction on the Abdominal Biomechanics: A Numerical Investigation," Comput. Methods Biomech. Biomed. Eng., **22**(2), pp. 139–148.

[39] Blanc, F. X., Coirault, C., Salmeron, S., Chemla, D., and Lecarpentier, Y., 2003, "Mechanics and Crossbridge Kinetics of Tracheal Smooth Muscle in Two Inbred Rat Strains," Eur. Respir. J., **22**(2), pp. 227–234.

[40] Klotz, T., Bleiler, C., and Röhrle, O., 2021, "A Physiology-Guided Classification of Active-Stress and Active-Strain Approaches for Continuum-Mechanical Modeling of Skeletal Muscle Tissue," Front Physiol., **12**(2021), p. 685531.

[41] Göktepe, S., Menzel, A., and Kuhl, E., 2014, "The Generalized Hill Model: A Kinematic Approach Towards Active Muscle Contraction," J. Mech. Phys. Solids, **72**(1), pp. 20–39.

[42] Murtada, S. I., Kroon, M., and Holzapfel, G. A., 2010, "A Calcium-Driven Mechanochemical Model for Prediction of Force Generation in Smooth Muscle," Biomech. Model Mechanobiol., **9**(6), pp. 749–762.

[43] Stålhand, J., Klarbring, A., and Holzapfel, G. A., 2011, "A Mechanochemical 3D Continuum Model for Smooth Muscle Contraction Under Finite Strains," J. Theor. Biol., **268**(1), pp. 120–130.